ACS Photonics

pubs.acs.org/journal/apchd5

Letter

Inverse Design of Lightweight Broadband Reflector for Relativistic Lightsail Propulsion

Weiliang Jin, Wei Li, Meir Orenstein, and Shanhui Fan*

Cite This: *ACS Photonics* 2020, 7, 2350−2355

Read Online

ACCESS | Metrics & More | Article Recommendations | Supporting Information

ABSTRACT: Light can exert forces on objects, promising to propel a meter-scale lightsail to near the speed of light. The key to address many challenges in such an ambition hinges on the nanostructuring of lightsails to tailor their optical scattering properties. In this Letter, we present a comprehensive study of photonic design of lightsails by applying large-scale optimization techniques to a generic geometry based on stacked photonic crystal layers. The optimization is performed by rigorous coupled-wave analysis amended with automatic differentiation methods for adjoint-variable gradient evaluations. Employing these methods, the propulsion efficiency of a lightsail that involves a trade-off between high broadband reflectivity and mass reduction is optimized. Surprisingly, regardless of the material choice, the optimal structures turn out to be simply one-dimensional subwavelength gratings, exhibiting nearly 50% improvement in acceleration distance performance compared to prior studies. Our framework can be extended to address other lightsail challenges such as thermal management and propulsion stability and applications in integrated photonics such as compact mirrors.

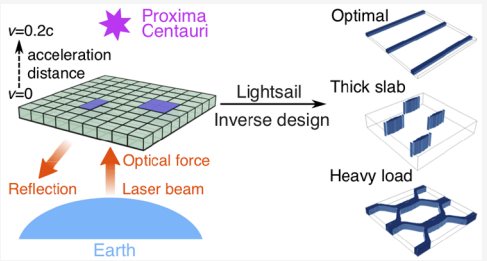

KEYWORDS: *inverse design, lightsail, optical force, photonic crystal, broadband mirror*

Light can exchange momentum with objects,[1] leading to many vital breakthroughs in the field of nanotechnology, such as optical tweezers for precise manipulation of nanoscale particles.[2,3] Optical force can also play a crucial role in much larger length scale applications such as space travel, including the recent launch of a solar sail driven by sun light.[4] Another and even more ambitious project is the Starshot Breakthrough Initiative that aims to accelerate a meter-size spacecraft to 20% of the speed of light, so that it can reach the nearby galaxy Proxima Centauri in 20 years.[5,6] By far, the most plausible propulsion mechanism is based on optical force[7] or radiation pressure from GW/m^2 level lasers.[8]

While such a project requires multidisciplinary efforts[6] such as materials science,[9] mechanical engineering, astrophysics,[10] and telecommunications,[11] many key challenges can be alleviated via probing the boundary of photonic design, including efficient propulsion,[8] heat management,[12] laser beam focusing,[13] and self-stabilization.[14−17] They all contain many trade-offs that were so far optimized by tuning few geometric parameters of simple photonic structures, leaving possibly much room for improvement by systematically studying more complicated structures. An important tool for accomplishing this task is inverse design method capable of exploring millions of design variables that have been introduced into photonics in the past decade,[18,19] proving to be powerful in discovering structures with performances that hit theoretical bounds[20] or in suggesting the existence of tighter fundamental limits, for example, recently improved bounds on optical absorption and scattering cross sections,[21] optical force,[22] near-field,[23,24] and far-field thermal radiation.[25]

In this Letter, as an initial step toward systemically pushing forward photonics-related performance of lightsails, we apply large-scale optimization methods to identify lightsail geometric design criteria for optimal propulsion efficiency, crucial to lowering both laser power and phase array size.[12] More specifically, we seek to minimize a figure-of-merit (FOM) described by eq 1, known as acceleration distance that involves a trade-off between broadband reflectivity and lightsail mass. Previous optimizations were based on simple photonic crystal (PhC) slabs,[8,12] in contrast, here we explore a generic class of geometries, stacked PhC layers whose dielectric spatial profiles can be arbitrarily set within the unit cell. Gradient-based optimization methods are applied to simultaneously optimize over dielectric distributions, periodicity of PhC, and thickness of each layer, whose gradients are conveniently evaluated with automatic differentiation methods.[26] Different constituent materials of lightsails and payload mass are studied. Surprisingly, we demonstrate that, for both high-index material such as silicon, and lower-index material such as silicon nitride, the optimal structure for a linearly polarized laser beam converges to a one-dimensional (1D) subwavelength grating, a robust solution for a wide range of payload mass. The FOM of

Received: May 10, 2020
Published: July 29, 2020

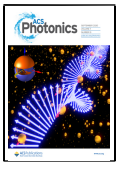

https://dx.doi.org/10.1021/acsphotonics.0c00768
ACS Photonics 2020, 7, 2350−2355

this optimal structure exhibits a nearly 50% improvement against that of previously explored structures. The enhancement is attributed to the destructive interference of two guided modes that can be supported in such a grating of small material volume filling ratio and at a subwavelength thickness. The optimal solutions can converge to more complicated two-dimensional (2D) PhC structures when more emphasis is imposed on maximizing reflectivity, for example, when the payload mass is large. Finally, we conclude that, in general, with optimizations, high-index material yields better performance.

In a general context, a broadband mirror is traditionally realized with a metallic reflector, which nevertheless possesses significant material absorption loss, incompatible with the thermal management requirement of the Starshot projects.[8] Recent advances in nanotechnologies have led to the development of low-loss all-dielectric mirrors, such as the distributed Bragg reflector[27] and several more compact schemes. One representative class of structures is derived from metamaterial principles by exploiting the single-negative response, commonly implemented with a single layer of microspheres, cubes,[28−30] or shapes discovered by using machine learning methods.[31] Another direction is based on guided-wave analysis that employs the double-mode destructive interference effect, realized with a subwavelength 1D grating of high-index contrast dielectrics.[32,33] The mechanism of the latter two approaches can be unified.[34] However, a comprehensive study on the mirror design principle for minimal mass is missing, a principle relevant in many integrated photonic applications and in efficient propulsion of lightsails.

As shown in Figure 1, we envision a spacecraft consisting of a payload (not shown) and a lightsail, where the latter is

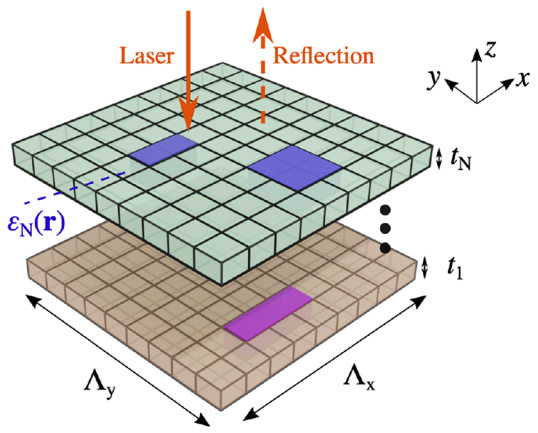

Figure 1. Schematic of a lightsail propelled by laser beams. The lightsail consists of stacked photonic crystal layers of period $\Lambda_{x(y)}$. The design space includes the period $\Lambda_{x(y)}$, the in-plane dielectric index value $\varepsilon_i(\mathbf{r})$ at each grid point, and the thickness t_i of the i-th layer. Here, different colors represent different materials.

structured to enhance the optical force along the normal $(-z)$ direction exerted on the sail by an incident high-power laser beam. From momentum conservation, the optical force increases with lightsail's reflectivity.[12,35] A practical FOM characterizing the propulsion efficiency is the distance D for the spacecraft to be accelerated to a target velocity, which takes into account the trade-off between optical force and kinetic quantities such as mass, which is captured by the following equation:[7,8]

$$D = \frac{c^3}{2I}(\rho_l + \rho_s)\int_0^{\beta_f} d\beta \frac{h(\beta)}{R[\lambda(\beta)]} \quad (1)$$

where $\rho_{s(l)}$ is the area density mass of the lightsail (payload), I is the laser intensity, c is the speed of light, and $h(\beta) = \beta/(1-\beta)^2\sqrt{1-\beta^2}$ encodes relativistic factors depending on velocity fraction $\beta = v/c$. The integration is performed from stationary motion to a target velocity $c\beta_f$, and during this time interval, the laser wavelength λ in the lightsail frame is Doppler red-shifted from λ_0 to $\lambda(\beta) = \lambda_0\sqrt{(1+\beta)/(1-\beta)}$. A representative value as in the Starshot project is $\beta_f = 0.2$, and consequently $\lambda(\beta_f) \approx 1.22\lambda_0$, revealing that the reflectivity R of the lightsail needs to be enhanced over a large bandwidth. Minimization of D has a direct impact on reducing both the size of the laser phase array that needs to account for diffraction,[12] as well as the total power consumption.

OPTIMIZATION FORMULATION

To minimize D, we seek to structure the lightsail with wavelength or subwavelength features that tailor its optical scattering properties. Since the lightsail should involve two vastly different geometric scales, a macroscopic area ~10 m^2 and nanoscale thickness on the order of 100 nm, the suitable generic class of geometries is stacked PhC slabs. As shown in Figure 1, each layer i with thickness t_i is uniform along z-direction, and periodically structured in the xy-plane. Such a platform contains a rich library of geometries, including the aforementioned dielectric broadband mirrors and previously explored lightsail structures such as uniform slabs, multilayer stacks, and PhC pillars or holes.[8,12] Inverse design of more complicated geometries, such as aperiodic structures, including Moiré lattices and photonic quasicrystals for inherent broadband responses,[36] and curved surfaces for mechanical stability,[16] will be considered in a future work.

In order to probe the limit of D via photonic designs, we apply the "topology" optimization approach[18] that enables us to explore the largest possible design space. More specifically, we discretize the unit cell of the i-th layer into $M_i \times M_i$ grids and allow to choose between materials at each grid point independently. This contributes to at least $\sum_{i=1}^{N} M_i^2$ design variables, each of which can take n discrete values, where N is the total number of layers, and n the number of candidate materials. We also treat the periodicity and the thickness of each layer as additional independent variables. The key to the tractability of such large-scale optimizations is the use of gradient-based optimization algorithms, such as the method of moving asymptotes (MMA).[37] To make use of these approaches, the index of refraction at each grid can initially vary continuously between various types of materials and, subsequently, be binarized with filter and regularization methods.[38] However, such local optimization algorithms are known to be ill-behaved over high-index dielectric structures[39] due to the presence of many narrow-band resonances, such as bound states in the continuum.[40] To better approach globally optimal solutions, we employ a relaxation method that broadens any high-Q response by adding fictitious material absorption loss to the entire system and eventually turning it off.[39] By employing this approach, our optimization can

https://dx.doi.org/10.1021/acsphotonics.0c00768
ACS Photonics 2020, 7, 2350−2355

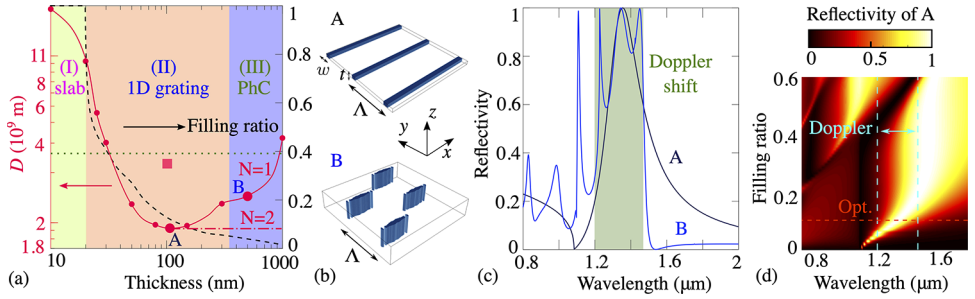

Figure 2. Inverse design of lightsail made of crystalline silicon. (a) acceleration distance D (left axis) and filling ratio (right axis) of single-layer structures ($N = 1$) optimized at several thicknesses (red dots) for a linearly polarized laser beam, illustrate the transition of optimal geometry from uniform slabs (green), one-dimensional gratings (orange), to two-dimensional PhCs (purple). The curves for D (red solid) and filling ratio (black dashed) are interpolated from the dots. Increasing the number of layers to $N = 2$ (red dash-dotted line) improves D at larger thickness. The ensemble averaged D over incidence polarization directions for the optimal polarization-insensitive structure (red square) is still better than that of the previous optimal design[8] (green dotted line). Two representative structures at points A and B are illustrated in (b), and their calculated reflection spectrum is shown in (c). The period of $A(B)$ is $\Lambda = 1.08(1.23)$ μm. Here the x-polarized laser beam is propagating along the z direction. (d) Reflectivity of the optimal grating A as a function of wavelength and width w or the filling ratio w/Λ. Typical Starshot parameters[8] are assumed: payload mass 0.1 g, lightsail area 10 m^2, and laser intensity 10 GW/m^2.

converge quickly within ~100 iterations (detailed in the Supporting Information), and the results are highly insensitive to initial parameters, a hint for possible globally optimal results.

The primary complexity of inverse design problems lies in the derivation of the adjoint-variable problem for efficient gradient evaluation.[18] While our FOM in eq 1 is simple, future work in optimizing other aspects of lightsails may lead to convoluted FOMs that makes the derivation of gradient information mind-twisting. Thankfully, recent advancement in machine learning community has led to the development of various convenient packages for automatic differentiation, the application of adjoint-variable methods to arbitrary computational graphs.[26] With those tools, we only need to implement forward problems, while the backward gradient evalulations will be generated automatically. For efficient optimization of eq 1 over arbitrarily structured PhC layers, we have implemented a package[41] that extends rigorous coupled-wave analysis (RCWA)[42] with the automatic differentiation software Autograd.[43]

RESULTS

We apply the optimization formulation to identify the optimal structuring criteria that minimize D. A glimpse at eq 1 indicates that the design criteria depends on the refractive indices of the constituent materials that dictate the scattering properties, and payload mass that governs the degree of trade-off between reflectivity and lightsail mass. To address those possibilities, we explore two types of dielectric materials of distinct refractive indices, as well as various values of payload mass. Without further specification, we assume typical Starshot parameters in which a laterally uniform laser beam of intensity 10 GW/m^2 and wavelength $\lambda_0 = 1.2$ μm is incident normally on a lightsail of area 10 m^2. The polarization of the laser is assumed to be linear, which is a typical laser configuration and is widely adopted in the lightsail designs.[14,15,17] To allow large design space, we consider a fine grid size $\lesssim$10 nm, leading to at least 10^4 spatial design variables per 1 μm^2 in each layer. We consider two choices of material on each grid point: the target material and a vacant space with unity refractive index and negligible mass, which in practice can be vacuum or aerogels.[44] In case of vacuum, a low-index substrate is needed for mechanical rigidity, which can be treated as payload mass. The dielectric dispersion of involved materials[45,46] is accounted for in evaluating eq 1.

We begin by studying the optimizations of a representative high-index material, crystalline silicon.[45] To gain insights into optimization results, we start by treating the overall thickness as a hyperparameter, namely, optimizing over period and material distributions at each thickness independently. The FOM (red solid line) and material volume filling ratio (black dashed line) of the optimal single-layer structures ($N = 1$) are depicted in Figure 2a, uncovering three distinct regimes of structural choices. First, at a small thickness $\lesssim$20 nm, as may be expected, the optimization converges to a finite-thickness uniform slab (green region) since at deep subwavelength thicknesses, the reflectivity of high-index material increases more steeply than mass with filling ratio.

Second, for the intermediate thickness range we obtain the best solution among our optimization results. Surprisingly, even though we are optimizing material distributions on 2D grids, the optimal shape is a 1D grating (orange region), depicted in the upper Figure 2b. With increasing thickness that allows for enhanced scattering, the optimal filling ratio, w/Λ, decreases in favor of lighter mass, with simultaneously enhanced average reflectivity in the Doppler-shift bandwidth, resulting in dramatically decreasing D that exhibits a minimum at thickness 107 nm (denoted as grating A in Figure 2a). Furthermore, we observe that, while the optimal period Λ also varies with thickness, it is always subwavelength $<\lambda_0$, for example, $\Lambda = 1.08$ μm, for grating A. Such a subwavelength grating eliminates the diffraction in off-normal directions, which is important for enhancing the optical force along the normal direction. Compared to previously explored structures,[8] the acceleration distance of grating A is $D_{Si} \approx 1.9 \times 10^9$ m, which represents a nearly 50% improvement. Additionally, we notice that it is straightforward to generalize grating A to the optimal polarization-insensitive solution, which turns out to be approximately a superposition of two 1D gratings along the two lateral directions (detailed in the Supporting Information). However, its ensemble averaged D over incidence polarization directions (red square in Figure 2a) is larger than the D of grating A, highlighting that orientation control of lightsails for polarization-locking[14] can improve propulsion efficiency.

https://dx.doi.org/10.1021/acsphotonics.0c00768
ACS Photonics 2020, 7, 2350−2355

In another context, 1D gratings have been proposed as broadband reflectors, known as high-contrast subwavelength gratings.[32] They have been demonstrated to achieve nearly 100% reflection over a bandwidth $\Delta\lambda/\lambda \gtrsim 30\%$ for either TE or TM polarized light, arising from the destructive interference of two guided modes that prohibits transmission. We examine if similar mechanism is the source of the performance of our optimized grating A by plotting its reflection spectrum in Figure 2c. A Fano resonance feature is visible near the Doppler shift range, demonstrating that the high broadband reflectivity is indeed attributed to the double-mode interference effects. Another important observation is that for the incident light polarized along the x-axis, denoted in Figure 2b, the algorithm always finds a grating extending along the same x-direction. This is consistent with previous studies[33] that gratings parallel to the light polarization direction, when compared to those of perpendicular orientations, can achieve broadband reflection with smaller filling ratio and, consequently, lighter mass. To gain more insights into the optimization process, in Figure 2d, we show the reflectivity plot of grating A as a function of wavelength and filling ratio for a fixed thickness and period. Indeed, high reflection mostly occurs in the nondiffractive region, $\lambda > \Lambda$. As the filling ratio decreases, the bandwidth of the high reflection region shrinks, a typical trade-off between the mass and average reflectivity. To minimize D, the algorithm compromises on a minimal filling ratio (red dashed line in Figure 2d) that does not degrade the reflectivity significantly. The $h(\beta)$-weighted average reflection at the optimal filling ratio is around 75%.

Third, at even larger thickness, the emphasis shifts to minimizing the volume filling ratio for mass reduction, as there is little room for further improvement of reflectivity that is bounded by 100%. Consequently, the optimal single-layer structure switches to more complicated 2D PhC structures (blue region). For example, the optimal geometry at thickness 500 nm, denoted as structure B and depicted in the lower Figure 2b, is a hexagonal lattice that resembles a trimmed 1D grating, a clear indication of the tendency of mass reduction. Its reflection spectrum, as shown in Figure 2c, reveals the presence of multiple resonance peaks within the Doppler-shift bandwidth, contributing to the slightly larger average reflection than that of grating A. Numerically, we find that compared to grating A, structure B exhibits only ~10% improvement of the average reflection, but nearly 70% reduction in volume filling ratio.

Another possibility of further improving the FOM is to explore multilayer structures ($N \gtrsim 2$). The FOM of the optimal double-layer structures ($N = 2$) as a function of overall thickness is shown in Figure 2a, the red dash-dotted curve. For overall thickness smaller than that of grating A, the optimization converges to the single-layer solution of the same thickness; at larger overall thickness, interestingly, it converges to grating A by setting one layer to be vacant and the other layer the same as grating A, leading to the flattening of the FOM curve at those thicknesses. We have applied the design also for $N = 3$ and 4, but obtained the same structures as for $N = 2$. Therefore, even with multiple independent layers, the optimal solution is simple 1D grating. We also want to emphasize that those inverse designed structures are mostly robust to perturbations, as they do not rely on high-Q resonances (detailed in Supporting Information).

Next we aim to generalize the above design criteria to other values of payload mass. At each value of payload mass, we simultaneously optimize over material distributions, period, and thickness. In the optimization, the thickness can vary between [0, 500] nm, and the period between [0, $3\lambda_0$]. The FOM of the optimal structures (red dots), grating A (blue solid curve), and the ideal massless perfect reflector (black dashed line) are compared in Figure 3. Over a wide range of

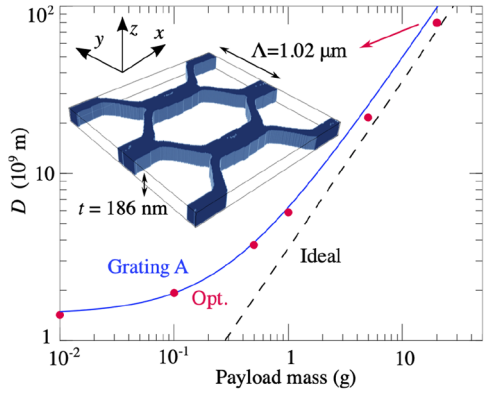

Figure 3. Acceleration distance as a function of payload mass for optimized structures (red dots), grating A of Figure 2 optimized for a payload mass 0.1 g (blue solid line), and ideal massless perfect reflector (black dashed line). Inset: the optimal structure for a payload mass 20 g.

payload mass, the FOM of grating A turns out to be very close to the optimal design, demonstrating that the simple 1D grating is a widely applicable optimal solution. For a large payload mass, the mass of the sail becomes less significant and the FOM depends almost entirely on the reflectivity, thus favoring structures of near-perfect reflection. For instance, for a payload mass of 20 g, the optimal structure is a honeycomb lattice (inset), whose average reflectivity approaches 95%.

Finally, we apply these optimization techniques to a lower-index constituent material, silicon nitride[46] for its appealing mechanical properties.[9] Different structural choice is expected as lower-index medium reflects light more weakly. As shown in Figure 4a, the optimal structure is exclusively a 1D grating (orange region) throughout the entire range of thickness [10, 1000] nm. The reason for ruling out the two other shapes as

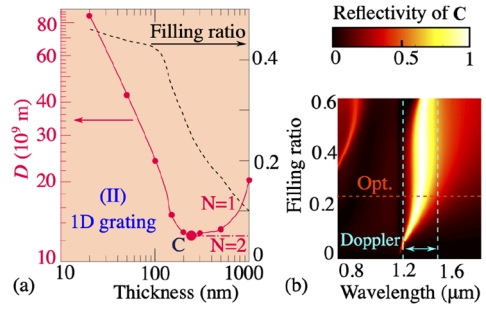

Figure 4. Inverse design of lightsail made of silicon nitride. (a) Acceleration distance (left axis) and filling ratio (right axis) of single-layer structures ($N = 1$) optimized at several thicknesses (red dots), illustrate that, over the entire range, the optimal geometry is a one-dimensional grating (orange). Increasing the number of layers to $N = 2$ (red dash-dotted line) improves D at larger thickness. (b) Reflectivity of the optimal grating structure C as a function of the filling ratio (w/Λ) and wavelength.

https://dx.doi.org/10.1021/acsphotonics.0c00768
ACS Photonics 2020, 7, 2350−2355

optimal solutions is as follows: at deep subwavelength thicknesses, reflection increases less dramatically than mass with filling ratio so that the uniform slabs that obtained for the high index material are not viable optimized solution here; at larger thicknesses, there is still much room for improvement of reflectivity, eliminating the need of cutting down on mass with 2D structuring. The overall optimal solution, denoted as grating *C*, occurs at a larger thickness, 243 nm, with a subwavelength period of $\Lambda = 1.17\ \mu$m. Its reflectivity plot as a function of wavelength and filling ratio is shown in Figure 4b, exhibiting a narrower high-reflectivity band than the silicon medium. Therefore, similar compromise is made to decide on a minimal filling ratio, resulting in a moderate average reflection 57% and larger acceleration distance $D_{SiN} \approx 13 \times 10^9$ m. The degraded FOM might also be attributed to the large mass density of silicon nitride, which is around 35% higher than that of silicon. We examine this possibility by optimizing over a fictitious silicon nitride with the same mass density of silicon. The optimal structure is found to be almost identical to that of the real silicon nitride, which leads to only slightly improved $D \approx D_{SiN}/1.35$, suggesting that the refractive index plays a more significant role.

CONCLUSION

We have developed an optimization framework that can effectively uncover optimal structure criteria for efficient lightsail propulsion. Under typical Starshot parameters, the lightsail geometry obtained by employing our optimization is a 1D subwavelength grating that outperforms the FOM of previous optimal structures by almost 50%. To ensure that we approach the globally optimal solutions, we expect future work on deriving a tight theoretical bound with methods such as Lagrange duality and energy conservation relations.[21] We envision that our optimization framework can be further applied to other challenges in the lightsail project, including thermal management,[12] polarization-locking,[14] and propulsion stability.[14,15]

ASSOCIATED CONTENT

Supporting Information

The Supporting Information is available free of charge at https://pubs.acs.org/doi/10.1021/acsphotonics.0c00768.

Additional information on optimization process, the optimal polarization-insensitive structure, and sensitivity analysis (PDF)

AUTHOR INFORMATION

Corresponding Author

Shanhui Fan − *Department of Electrical Engineering, Ginzton Laboratory, Stanford University, Stanford, California 94305, United States;* orcid.org/0000-0002-0081-9732; Email: shanhui@stanford.edu

Authors

Weiliang Jin − *Department of Electrical Engineering, Ginzton Laboratory, Stanford University, Stanford, California 94305, United States;* orcid.org/0000-0003-1946-1029

Wei Li − *Department of Electrical Engineering, Ginzton Laboratory, Stanford University, Stanford, California 94305, United States;* orcid.org/0000-0002-2227-9431

Meir Orenstein − *Department of Electrical Engineering, Technion-Israel Institute of Technology, 32000 Haifa, Israel*

Complete contact information is available at: https://pubs.acs.org/10.1021/acsphotonics.0c00768

Notes

The authors declare no competing financial interest.

ACKNOWLEDGMENTS

We would like to thank Dr. Zin Lin, Dr. Ian Williamson, Dr. Momchil Minkov, Dr. Viktar Asadchy, Dr. Bo Zhao, and Cheng Guo for useful discussions. This work is supported by the Breakthrough Starshot Initiative (initial idea and performance testing), and the U.S. Department of Energy "Photonics at Thermodynamic Limits" Energy Frontier Research Center under Grant No. DE-SC0019140 (theoretical modeling), and used the Extreme Science and Engineering Discovery Environment (XSEDE) supported by the National Science Foundation, at the San Diego Supercomputing Center through allocation TG-MCA03S007.

REFERENCES

(1) Novotny, L.; Hecht, B. *Principles of Nano-Optics*; Cambridge University Press, 2012.

(2) Moffitt, J. R.; Chemla, Y. R.; Smith, S. B.; Bustamante, C. Recent advances in optical tweezers. *Annu. Rev. Biochem.* **2008**, *77*, 205−228.

(3) Gao, D.; Ding, W.; Nieto-Vesperinas, M.; Ding, X.; Rahman, M.; Zhang, T.; Lim, C.; Qiu, C.-W. Optical manipulation from the microscale to the nanoscale: fundamentals, advances and prospects. *Light: Sci. Appl.* **2017**, *6*, e17039−e17039.

(4) Mansell, J.; Spencer, D. A.; Plante, B.; Diaz, A.; Fernandez, M.; Bellardo, J.; Betts, B.; Nye, B. Orbit and attitude performance of the LightSail 2 solar sail spacecraft. *AIAA Scitech 2020 Forum* **2020**, 2177.

(5) Lubin, P. A Roadmap to Interstellar Flight. *JBIS* **2016**, *69*, 40−72.

(6) Parkin, K. L. The breakthrough starshot system model. *Acta Astronaut.* **2018**, *152*, 370−384.

(7) Kulkarni, N.; Lubin, P.; Zhang, Q. Relativistic spacecraft propelled by directed energy. *Astronomical Journal* **2018**, *155*, 155.

(8) Atwater, H. A.; Davoyan, A. R.; Ilic, O.; Jariwala, D.; Sherrott, M. C.; Went, C. M.; Whitney, W. S.; Wong, J. Materials challenges for the Starshot lightsail. *Nat. Mater.* **2018**, *17*, 861.

(9) Moura, J. P.; Norte, R. A.; Guo, J.; Schäfermeier, C.; Gröblacher, S. Centimeter-scale suspended photonic crystal mirrors. *Opt. Express* **2018**, *26*, 1895−1909.

(10) Lingam, M.; Loeb, A. Propulsion of spacecrafts to relativistic speeds using natural astrophysical sources. *ApJ* **2020**, *894*, 36.

(11) Bird, J.; Petzold, L.; Lubin, P.; Deacon, D. Advances in deep space exploration via simulators and deep learning. *arXiv:2002.04051 [astro-ph.IM]* **2020**, na.

(12) Ilic, O.; Went, C. M.; Atwater, H. A. Nanophotonic heterostructures for efficient propulsion and radiative cooling of relativistic light sails. *Nano Lett.* **2018**, *18*, 5583−5589.

(13) Noyes, M.; Hart, M. Analyzing the viability of Satellite Laser Guide Stars for Breakthrough Starshot. Proc. AO4ELT6, The University of Arizona, 2019; na; http://ao4elt6.copl.ulaval.ca/proceedings/401-CqJr-251.pdf.

(14) Ilic, O.; Atwater, H. A. Self-stabilizing photonic levitation and propulsion of nanostructured macroscopic objects. *Nat. Photonics* **2019**, *13*, 289.

(15) Siegel, J.; Wang, A. Y.; Menabde, S. G.; Kats, M. A.; Jang, M. S.; Brar, V. W. Self-stabilizing laser sails based on optical metasurfaces. *ACS Photonics* **2019**, *6*, 2032−2040.

(16) Manchester, Z.; Loeb, A. Stability of a light sail riding on a laser beam. *Astrophys. J., Lett.* **2017**, *837*, L20.

(17) Myilswamy, K. V.; Krishnan, A.; Povinelli, M. L. Photonic crystal lightsail with nonlinear reflectivity for increased stability. *Opt. Express* **2020**, *28*, 8223−8232.

(18) Molesky, S.; Lin, Z.; Piggott, A. Y.; Jin, W.; Vucković, J.; Rodriguez, A. W. Inverse design in nanophotonics. *Nat. Photonics* **2018**, *12*, 659−670.
(19) Yao, K.; Unni, R.; Zheng, Y. Intelligent nanophotonics: merging photonics and artificial intelligence at the nanoscale. *Nanophotonics* **2019**, *8*, 339−366.
(20) Angeris, G.; Vuckovic, J.; Boyd, S. P. Computational bounds for photonic design. *ACS Photonics* **2019**, *6*, 1232−1239.
(21) Molesky, S.; Chao, P.; Jin, W.; Rodriguez, A. W. T-operator limits on electromagnetic scattering: bounds on extinguished, absorbed, and scattered power from arbitrary sources. *Phys. Rev. Research* **2020**, *2*, 033172.
(22) Lee, Y. E.; Miller, O. D.; Reid, M. H.; Johnson, S. G.; Fang, N. X. Computational inverse design of non-intuitive illumination patterns to maximize optical force or torque. *Opt. Express* **2017**, *25*, 6757−6766.
(23) Venkataram, P. S.; Molesky, S.; Jin, W.; Rodriguez, A. W. Fundamental limits to radiative heat transfer: the limited role of nanostructuring in the near-field. *Phys. Rev. Lett.* **2020**, *124*, 013904.
(24) Jin, W.; Molesky, S.; Lin, Z.; Rodriguez, A. W. Material scaling and frequency-selective enhancement of near-field radiative heat transfer for lossy metals in two dimensions via inverse design. *Phys. Rev. B: Condens. Matter Mater. Phys.* **2019**, *99*, 041403.
(25) Molesky, S.; Jin, W.; Venkataram, P. S.; Rodriguez, A. W. T operator bounds on angle-integrated absorption and thermal radiation for arbitrary objects. *Phys. Rev. Lett.* **2019**, *123*, 257401.
(26) Minkov, M.; Williamson, I. A.; Andreani, L. C.; Gerace, D.; Lou, B.; Song, A. Y.; Hughes, T. W.; Fan, S. Inverse design of photonic crystals through automatic differentiation. *ACS Photonics* **2020**, *7*, 1729−1741.
(27) Coldren, L. A. Diode lasers and photonic integrated circuits. *Opt. Eng.* **1997**, *36*, 616.
(28) Slovick, B.; Yu, Z. G.; Berding, M.; Krishnamurthy, S. Perfect dielectric-metamaterial reflector. *Phys. Rev. B: Condens. Matter Mater. Phys.* **2013**, *88*, 165116.
(29) Moitra, P.; Slovick, B. A.; Gang Yu, Z.; Krishnamurthy, S.; Valentine, J. Experimental demonstration of a broadband all-dielectric metamaterial perfect reflector. *Appl. Phys. Lett.* **2014**, *104*, 171102.
(30) Moitra, P.; Slovick, B. A.; Li, W.; Kravchencko, I. I.; Briggs, D. P.; Krishnamurthy, S.; Valentine, J. Large-scale all-dielectric metamaterial perfect reflectors. *ACS Photonics* **2015**, *2*, 692−698.
(31) Harper, E. S.; Coyle, E. J.; Vernon, J. P.; Mills, M. S. Inverse design of broadband highly reflective metasurfaces using neural networks. *Phys. Rev. B: Condens. Matter Mater. Phys.* **2020**, *101*, 195104.
(32) Mateus, C. F.; Huang, M. C.; Deng, Y.; Neureuther, A. R.; Chang-Hasnain, C. J. Ultrabroadband mirror using low-index cladded subwavelength grating. *IEEE Photonics Technol. Lett.* **2004**, *16*, 518−520.
(33) Karagodsky, V.; Sedgwick, F. G.; Chang-Hasnain, C. J. Theoretical analysis of subwavelength high contrast grating reflectors. *Opt. Express* **2010**, *18*, 16973−16988.
(34) Ko, Y. H.; Magnusson, R. Wideband dielectric metamaterial reflectors: Mie scattering or leaky Bloch mode resonance? *Optica* **2018**, *5*, 289−294.
(35) Chen, J.; Ng, J.; Lin, Z.; Chan, C. Optical pulling force. *Nat. Photonics* **2011**, *5*, 531−534.
(36) Dal Negro, L. *Optics of Aperiodic Structures: Fundamentals and Device Applications*; CRC Press, 2013.
(37) Svanberg, K. A class of globally convergent optimization methods based on conservative convex separable approximations. *SIAM journal on optimization* **2002**, *12*, 555.
(38) Jensen, J. S.; Sigmund, O. Topology optimization for nano-photonics. *Laser & Photonics Reviews* **2011**, *5*, 308−321.
(39) Liang, X.; Johnson, S. G. Formulation for scalable optimization of microcavities via the frequency-averaged local density of states. *Opt. Express* **2013**, *21*, 30812−30841.
(40) Hsu, C. W.; Zhen, B.; Stone, A. D.; Joannopoulos, J. D.; Soljačić, M. Bound states in the continuum. *Nature Reviews Materials* **2016**, *1*, 1−13.
(41) Jin, W. gRCWA: rigorous coupled wave analysis supporting automatic differentation with autograd; https://github.com/weiliangjinca/grcwa.
(42) Liu, V.; Fan, S. S4: A free electromagnetic solver for layered periodic structures. *Comput. Phys. Commun.* **2012**, *183*, 2233−2244.
(43) *Autograd: Efficiently computes derivatives of numpy code*; Available at https://github.com/HIPS/autograd.
(44) Jo, M.-H.; Hong, J.-K.; Park, H.-H.; Kim, J.-J.; Hyun, S.-H.; Choi, S.-Y. Application of SiO2 aerogel film with low dielectric constant to intermetal dielectrics. *Thin Solid Films* **1997**, *308*, 490−494.
(45) Palik, E. D. *Handbook of Optical Constants of Solids*; Academic Press, 1998; Vol. 3.
(46) Luke, K.; Okawachi, Y.; Lamont, M. R.; Gaeta, A. L.; Lipson, M. Broadband mid-infrared frequency comb generation in a Si_3N_4 microresonator. *Opt. Lett.* **2015**, *40*, 4823−4826.

https://dx.doi.org/10.1021/acsphotonics.0c00768
ACS Photonics 2020, 7, 2350−2355